Geometry-Driven Stochastic Modeling of SE(3) States Based on Dual Quaternion Representation

Kailai Li, **Florian Pfaff**, and **Uwe D. Hanebeck**
Intelligent Sensor-Actuator-Systems Laboratory (ISAS)
Institute for Anthropomatics and Robotics
Karlsruhe Institute of Technology (KIT), Germany
kailai.li@kit.edu, florian.pfaff@kit.edu, uwe.hanebeck@ieee.org

***Abstract*—We present a novel approach to stochastically model uncertain 6-DoF rigid body motions represented by dual quaternions. Unlike conventional methods relying on the local linearization of the nonlinear SE(3) group, the proposed distribution directly models uncertainty on the manifold of unit dual quaternions. For that, the Bingham distribution is employed on the 3-sphere to model the real part, at which the tangent plane of the hypersphere is spanned by a basis preserving the Bingham principal directions via parallel transport. The conditioning dual part is then expressed with respect to the transported basis and modeled by a Gaussian distribution. This enables the probabilistic interpretation of the correlation between rotation and translation terms. We further introduce the corresponding sampling-approximation scheme for the proposed density, based on which unscented transform-based 6-DoF pose filtering approaches are established and evaluated with simulations.**

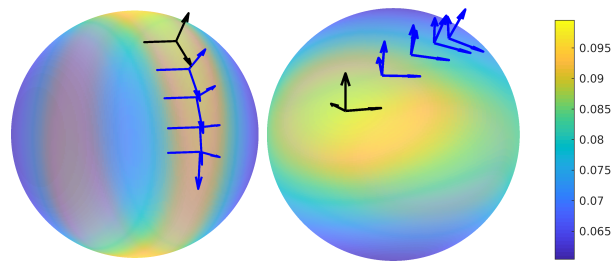

Fig. 1: Examples of basis parallel transport [15] on $\mathbb{S}^2$ sphere. Here, Bingham distributions of two different parameters are defined on the sphere (color bar indicates density). Basis in accordance of the principal directions at the mode (black coordinates) are transported along certain geodesic curves. The parallel transport enables two vectors on different spherical tangent planes to be parallel with respect to the geodesic curve between them.

I. Introduction

Recursive pose estimation plays a fundamental role in various robotic tasks such as localization [1], scene registration [2], and perception [3], as well as autonomous locomotion and manipulation [4]. Due to the nonlinear structure of the special Euclidean group SE(3), stochastic modeling of uncertain 6-DoF poses is nontrivial. From the perspective of Lie groups, most existing methods rely on the local linearization of corresponding nonlinear manifolds (e.g., via Lie algebra), which are essentially approximations by assuming local perturbations [5]. However, linearizations can be risky if the system models entail large uncertainty and fast motion. In this case, higher-order motion information are usually needed and multi-sensor fusion techniques are required [6].

Moreover, spatial transformations can be parameterized in different ways, e.g., via Euler angles and translation terms, or the well-known 4×4 homogeneous matrices. However, the former one inherently brings ambiguities due to the *gimbal lock* issue. Homogeneous matrices guarantee unique representations through overparameterization, but can suffer from numerical instabilities caused by the large degree of redundancy. In contrast, dual quaternions can simultaneously represent orientations and rotations without ambiguity and with less redundancy (using 8 instead of 16 elements in homogeneous matrices for representing the 6 DoF).

Over the years, there has been much effort dedicated for stochastic modeling uncertain dual quaternions in the context of recursive pose estimation. As the extra two degrees of redundancy constrain the dual quaternion states on a nonlinear manifold embedded in the 8-dimensional Euclidean space, existing approaches normally model the uncertainty in a locally linearized space [7]. This can lead to poor robustness and accuracy as formerly discussed. Direct on-manifold modeling approaches have been first pioneered by [8], [9] for the orientation filtering: uncertain unit quaternions on the $\mathbb{S}^3$ hypersphere are modeled by the Bingham distribution without local linearization. In [10], [11], uncertain dual quaternions representing planar motions have been modeled via the Bingham-distributed real part with the conditioned Gaussian-distributed dual part. An extension towards 6-DoF recursive pose filtering based on the Bingham distribution was introduced in [12]. However, it is specifically targeted for static scene registration, where pseudo-measurements using paired points are required to formulate a linear filter setup. In [13], an unscented filtering framework has been proposed for vision-based simultaneous localization and mapping (SLAM) based on the dual quaternion representation. However, the stochastic modeling of the poses lacks probabilistic interpretation for the correlation between rotation and translation terms. In [14], the uncertainty of dual quaternions is modeled by a Gaussian distribution on the tangent plane of the hypersphere through projection. Unfortunately, applying it to Bayesian inference imposes the prerequisite of small orientation changes.

In this paper, a novel approach for modeling uncertain 6-DoF poses represented by unit dual quaternions is proposed. We employ the Bingham distribution on the $\mathbb{S}^3$ hypersphere to model the rotation quaternions. Taking the idea of Riemannian geometry, the Bingham principal directions at the mode can then be preserved on $\mathbb{S}^3$ via parallel transport and further serve as the local basis of the tangent plane on the hypersphere. Thus, the translation terms can be interpreted probabilistically with respect to the transported basis by a Gaussian distribution. Examples of basis parallel transport for Bingham distributions on $\mathbb{S}^2$ sphere are shown in Fig. 1. More specifically, our main contributions are:

- The uncertainty of 6-DoF rigid body motions are directly modeled on the manifold of unit dual quaternions without local linearization.
- The probabilistic correlation between rotation and translation terms is inherently considered based on hyperspherical parallel transport.
- A sampling-approximation scheme is proposed based on the novel density and further applied in the unscented transform-based recursive filtering framework.

The remainder of the paper is structured as follows. In Sec. II, preliminaries about dual quaternion pose representation and the Bingham distribution are introduced. The novel geometry-driven stochastic modeling of uncertain unit dual quaternions is introduced in Sec. III. The sampling-approximation scheme is proposed in Sec. IV, based on which the unscented transform-based Bayesian inference framework is established. Finally, the work is concluded in Sec. V.

II. Preliminaries

A. Parameterization of Spatial Rotations Using Quaternions

By convention, 3-DoF spatial rotations can be parameterized by quaternions in the following form [16]

$$\mathbf{x}_\mathrm{r} = \big[\cos(\theta/2),\, \mathbf{n}^\top \sin(\theta/2)\big]^\top \in \mathbb{R}^4\,, \tag{1}$$

with the unit vector $\mathbf{n} \in \mathbb{R}^3$ denoting the axis around which a rotation of angle θ is performed. The norm of quaternions is defined as $\|\mathbf{x}_\mathrm{r}\| = \sqrt{\mathbf{x}_\mathrm{r} \otimes \mathbf{x}_\mathrm{r}^*}$, with $\otimes$ being the Hamilton product [17] and $\mathbf{x}_\mathrm{r}^* = \mathrm{diag}(1,-1,-1,-1)\,\mathbf{x}_\mathrm{r}$ being the conjugate of $\mathbf{x}_\mathrm{r}$. Here, $\mathrm{diag}(\cdot)$ denotes a diagonal matrix with the entries given as diagonal elements. Therefore, the quaternions in (1) are of unit norm and also of unit length in $\mathbb{R}^4$, thus $\mathbf{x}_\mathrm{r} \in \mathbb{S}^3 \subset \mathbb{R}^4$. Given the unit quaternion defined in (1), a point $\mathbf{v} \in \mathbb{R}^3$ can be rotated to $\mathbf{v}'$ accordingly via

$$\big[\,0, \mathbf{v}'^\top\big]^\top = \mathbf{x}_\mathrm{r} \otimes \big[\,0,\, \mathbf{v}^\top\big]^\top \otimes \mathbf{x}_\mathrm{r}^*\,, \tag{2}$$

with $[\,0, \mathbf{v}^\top]^\top$ being the quaternion form of vector $\mathbf{v}$.

Moreover, the set of unit quaternions is closed under the Hamilton product, which essentially denotes 4-dimensional rotations on the $\mathbb{S}^3$ hypersphere. For instance, $\forall\, \mathbf{p} = [p_0, p_1, p_2, p_3]^\top$, $\mathbf{q} = [q_0, q_1, q_2, q_3]^\top \in \mathbb{S}^3$, their Hamilton product can be reformulated into ordinary matrix–vector multiplication, namely $\mathbf{p} \otimes \mathbf{q} = \mathbf{Q}_\mathbf{p}^{\llcorner}\, \mathbf{q} = \mathbf{Q}_\mathbf{q}^{\lrcorner}\, \mathbf{p}$, with

$$\mathbf{Q}_\mathbf{p}^{\llcorner} = \begin{bmatrix} p_0 & -p_1 & -p_2 & -p_3 \\ p_1 & p_0 & -p_3 & p_2 \\ p_2 & p_3 & p_0 & -p_1 \\ p_3 & -p_2 & p_1 & p_0 \end{bmatrix}, \quad \mathbf{Q}_\mathbf{q}^{\lrcorner} = \begin{bmatrix} q_0 & -q_1 & -q_2 & -q_3 \\ q_1 & q_0 & q_3 & -q_2 \\ q_2 & -q_3 & q_0 & q_1 \\ q_3 & q_2 & -q_1 & q_0 \end{bmatrix} \tag{3}$$

being the left and right matrix representation and $\mathbf{Q}_\mathbf{p}^{\llcorner}, \mathbf{Q}_\mathbf{q}^{\lrcorner} \in \mathrm{SO}(4)$ (proven in Appendix A). For unit quaternions, their inverse is identical to the conjugate, i.e., $\mathbf{q}^{-1} = \mathbf{q}^*$, with its matrix representation, either composed from left or right hand side, satisfying $\mathbf{Q}_{\mathbf{q}^{-1}} = \mathbf{Q}_\mathbf{q}^{-1} = \mathbf{Q}_\mathbf{q}^\top$ [16].

B. Dual Quaternion Parameterization of Rigid Body Motions

A dual quaternion is essentially a tuple of paired quaternions combined by the *dual unit* ϵ ($\epsilon^2 = 0$), namely $\mathbf{x} = \mathbf{x}_\mathrm{r} + \epsilon\, \mathbf{x}_\mathrm{d}$. Here, $\mathbf{x}_\mathrm{r}$ denotes the *real part* and $\mathbf{x}_\mathrm{d}$ the *dual part*. Concatenation of the real and dual part then results in the following vector form of dual quaternions[1] $\mathbf{x} = [\,\mathbf{x}_\mathrm{r}^\top,\, \mathbf{x}_\mathrm{d}^\top\,]^\top \in \mathbb{R}^8$. Thus, the arithmetics of dual quaternions is the combination of the Hamilton product and dual number theory. We use $\boxplus$ to denote the product of two dual quaternions (example shown in Appendix B). Multiplication of two dual quaternions can also be expressed as ordinary matrix–vector product [11]. For two dual quaternions $\mathbf{x} = [\,\mathbf{x}_\mathrm{r}^\top,\, \mathbf{x}_\mathrm{d}^\top\,]^\top$ and $\mathbf{y} = [\,\mathbf{y}_\mathrm{r}^\top,\, \mathbf{y}_\mathrm{d}^\top\,]^\top$, we have $\mathbf{x} \boxplus \mathbf{y} = \mathbf{Q}_\mathbf{x}^{\ulcorner}\, \mathbf{y} = \mathbf{Q}_\mathbf{y}^{\urcorner}\, \mathbf{x}$, with

$$\mathbf{Q}_\mathbf{x}^{\ulcorner} = \begin{bmatrix} \mathbf{Q}_{\mathbf{x}_\mathrm{r}}^{\llcorner} & \mathbf{0} \\ \mathbf{Q}_{\mathbf{x}_\mathrm{d}}^{\llcorner} & \mathbf{Q}_{\mathbf{x}_\mathrm{r}}^{\llcorner} \end{bmatrix}, \mathbf{Q}_\mathbf{y}^{\urcorner} = \begin{bmatrix} \mathbf{Q}_{\mathbf{y}_\mathrm{r}}^{\lrcorner} & \mathbf{0} \\ \mathbf{Q}_{\mathbf{y}_\mathrm{d}}^{\lrcorner} & \mathbf{Q}_{\mathbf{y}_\mathrm{r}}^{\lrcorner} \end{bmatrix}, \tag{4}$$

and $\mathbf{0} \in \mathbb{R}^{4\times 4}$. Furthermore, the norm of dual quaternions is defined as $\|\mathbf{x}\| = \sqrt{\mathbf{x} \boxplus \mathbf{x}^*}$, with $\mathbf{x}^* = [\,\mathbf{x}_\mathrm{r}^{*\top},\, \mathbf{x}_\mathrm{d}^{*\top}\,]^\top$ being the *classic conjugate* of $\mathbf{x}$, where the real and dual part are conjugated individually. By imposing unit norm constraints, the manifold of unit dual quaternions can be derived as

$$\Omega = \Big\{ \big[\,\mathbf{x}_\mathrm{r}^\top,\, \mathbf{x}_\mathrm{d}^\top\,\big]^\top \,\Big|\, \mathbf{x}_\mathrm{r} \in \mathbb{S}^3,\, \mathbf{x}_\mathrm{r}^\top \mathbf{x}_\mathrm{d} = 0 \Big\} \subset \mathbb{R}^8\,, \tag{5}$$

which indicates that the real part $\mathbf{x}_\mathrm{r}$ is located on the hypersphere $\mathbb{S}^3$ as given in (1) with the dual part $\mathbf{x}_\mathrm{d}$ being orthogonal to the real part. The derivation can be found in Appendix C.

Similar to unit quaternions parameterizing spatial rotations, dual quaternions of unit norm are a compact representation of rigid transformations fulfilling the two constraints in (5). By convention [12], the real part $\mathbf{x}_\mathrm{r}$ is defined as in (1) representing the rotations and the dual part is given as

$$\mathbf{x}_\mathrm{d} = \frac{1}{2}\big[\,0,\, \mathbf{t}^\top\big]^\top \otimes \mathbf{x}_\mathrm{r}\,, \tag{6}$$

with $\mathbf{t} \in \mathbb{R}^3$ being the translation, such that any $\mathbf{v} \in \mathbb{R}^3$ can be transformed to $\mathbf{v}'$ via

$$\big[\,1,0,0,0,0,\mathbf{v}'^\top\,\big]^\top = \mathbf{x} \boxplus \big[\,1,0,0,0,0,\mathbf{v}^\top\,\big]^\top \boxplus \mathbf{x}^\circ \tag{7}$$

(proof shown in Appendix D). Here, $[\,1,0,0,0,0,\mathbf{v}^\top\,]^\top$ denotes the dual quaternion form of vector $\mathbf{v}$ and $\mathbf{x}^\circ = [\,\mathbf{x}_\mathrm{r}^{*\top},\, -\mathbf{x}_\mathrm{d}^{*\top}\,]^\top$ is the *full conjugate* of $\mathbf{x}$ (both the dual unit and quaternion components are conjugated).

C. Stochastic Modeling of Uncertain Unit Quaternions

The Bingham distribution [18] on $\mathbb{S}^3$ is defined as

$$f_\mathcal{B}(\mathbf{x}_\mathrm{r}; \mathbf{Z}, \mathbf{M}) = \frac{1}{N_\mathcal{B}(\mathbf{Z})} \exp\left(\mathbf{x}_\mathrm{r}^\top \mathbf{M}\,\mathbf{Z}\,\mathbf{M}^\top \mathbf{x}_\mathrm{r}\right)\,, \tag{8}$$

with $\mathbf{Z} = \mathrm{diag}(z_1, z_2, z_3, z_0)$ being the concentration matrix controlling the dispersion, $N_\mathcal{B}(\mathbf{Z})$ the normalization constant, and real orthogonal matrix $\mathbf{M} \in \mathbb{R}^{4\times 4}$ indicating the principal directions of the density. As (2) shows, two antipodal unit quaternions on the hypersphere, i.e., $\mathbf{x}_\mathrm{r}, -\mathbf{x}_\mathrm{r} \in \mathbb{S}^3$, represent the same rotation. Thus, the Bingham distribution defined in (8) is well-suited to model the uncertainty of unit quaternions,

[1] For better readability in this paper, we use $\mathbf{x}$ to denote both the dual number form and the vector form of dual quaternions.

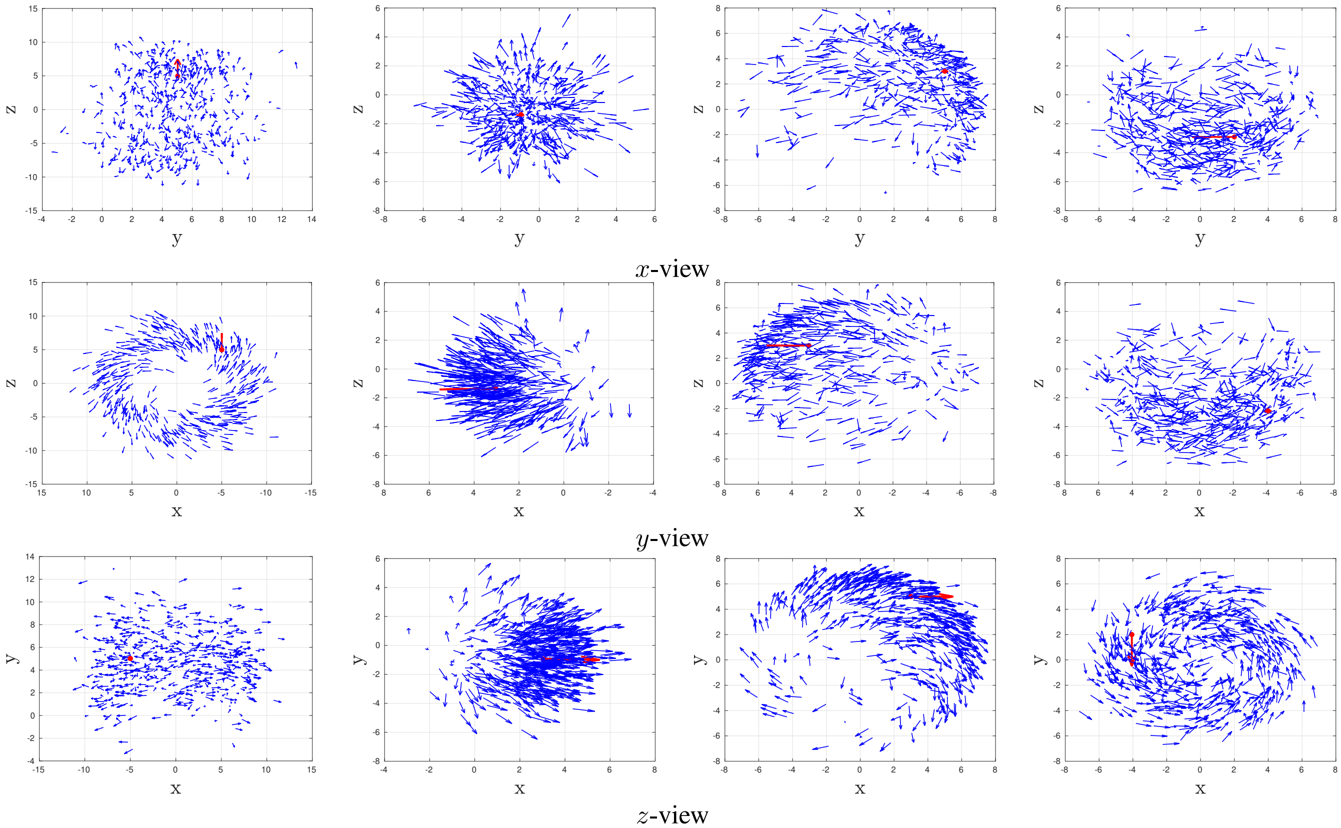

Fig. 2: Examples of random sampling from the proposed density via the sampling scheme introduced in Alg. 1 . Figures in each column visualize dual quaternion samples represented by 3-D poses of the same parameter configuration. Here, the blue arrows indicate random samples, whereas the red one gives the mode of the distribution.

as its density is antipodally symmetric on $\mathbb{S}^3$, i.e., $f_{\mathcal{B}}(\mathbf{x}_\mathrm{r}) = f_{\mathcal{B}}(-\mathbf{x}_\mathrm{r})$. Moreover, the parameter matrices $\mathbf{Z}$ and $\mathbf{M}$ can be derived via eigendecomposition of a negative semidefinite matrix $\mathbf{C}_{\mathcal{B}}$. Afterward, the eigenvalues in $\mathbf{Z}$ are by convention re-aligned in ascending order [9], i.e., $z_1 \leq z_2 \leq z_3 \leq z_0 \leq 0$, and the column vectors in $\mathbf{M}$ are re-ordered accordingly as $[\,\mathbf{m}_1, \mathbf{m}_2, \mathbf{m}_3, \mathbf{m}_0\,]$. The mode of the density can then be recognized as the column vector associated with the largest eigenvalue, namely $\mathbf{m}_0$.

III. On-manifold Stochastic Modeling for Uncertain Unit Dual Quaternions

A. Geometric Structure of the Unit Dual Quaternion Manifold

The unit dual quaternion manifold as introduced in (5) is compact and can be identified as a differentiable Riemannian manifold [19], [20]. Here, the dual part defined in (6) can be further reformulated via the matrix representation introduced in (3) as $\mathbf{x}_\mathrm{d} = 0.5\,\mathbf{Q}^{\lrcorner}_{\mathbf{x}_\mathrm{r}}[\,0,\, \mathbf{t}^\top\,]^\top = 0.5\,\mathbf{E}^{\lrcorner}_{\mathbf{x}_\mathrm{r}}\mathbf{t}$, with $\mathbf{E}^{\lrcorner}_\mathrm{r} \in \mathbb{R}^{4\times 3}$ being the last three columns of the matrix $\mathbf{Q}^{\lrcorner}_{\mathbf{x}_\mathrm{r}}$, namely $\mathbf{Q}^{\lrcorner}_{\mathbf{x}_\mathrm{r}} = [\,\mathbf{x}_\mathrm{r}, \mathbf{E}^{\lrcorner}_\mathrm{r}\,]$. As $\mathbf{Q}^{\lrcorner}_{\mathbf{x}_\mathrm{r}} \in \mathrm{SO}(4)$, the column vectors of matrix $\mathbf{E}^{\lrcorner}_{\mathbf{x}_\mathrm{r}}$ essentially provide an orthonormal basis spanning the tangent space of the hypersphere $\mathbb{S}^3$ at $\mathbf{x}_\mathrm{r}$, i.e., $\mathcal{T}_{\mathbf{x}_\mathrm{r}}\mathbb{S}^3 = \mathrm{span}\{\mathbf{e}_1, \mathbf{e}_2, \mathbf{e}_3\}$, with $\mathbf{E}^{\lrcorner}_\mathrm{r} = [\,\mathbf{e}_1, \mathbf{e}_2, \mathbf{e}_3\,]$. It can be easily proven that $\mathbf{E}^{\lrcorner\top}_\mathrm{r}\mathbf{E}^{\lrcorner}_\mathrm{r} = \mathbf{I} \in \mathbb{R}^{3\times 3}$. Thus the encapsulated pure translation in the dual part can be regenerated via $\mathbf{t} = 2\,\mathbf{E}^{\lrcorner\top}_\mathrm{r}\mathbf{x}_\mathrm{d}$.

On the other hand, given the Bingham distribution defined in (8), the tangent plane at the mode $\mathbf{m}_0$ can also be spanned by the first three column vectors of matrix $\mathbf{M}$, namely $\mathcal{T}_{\mathbf{m}_0}\mathbb{S}^3 = \mathrm{span}\,\{\mathbf{m}_1, \mathbf{m}_2, \mathbf{m}_3\}$, with $\{\mathbf{m}_1, \mathbf{m}_2, \mathbf{m}_3\}$ being the orthonormal basis. For simplicity of the derivation below, we denote $\mathbf{E}^\mathrm{B} = [\,\mathbf{m}_1, \mathbf{m}_2, \mathbf{m}_3\,]$, such that $\mathbf{M} = [\,\mathbf{E}^\mathrm{B},\, \mathbf{m}_0\,]$.

B. On-manifold Basis Parallel Transport

In order to probabilistically interpret the correlation between the translation term and the rotation quaternion, we decode the dual part $\mathbf{x}_\mathrm{d}$ located on the tangent plane $\mathcal{T}_{\mathbf{x}_\mathrm{r}}\mathbb{S}^3$ with respect to a basis that preserves the Bingham principal directions at $\mathbf{x}_\mathrm{r}$. For that, we employ the *parallel transport* technique from Riemannian geometry [15], [20] on $\mathbb{S}^3$ to shift the tangent plane coordinates at the mode $\mathbf{m}_0$ to $\mathbf{x}_\mathrm{r}$, namely

$$\mathbf{E}^\mathrm{B}_\mathrm{r} = \mathbf{Q}^{\llcorner}_{\mathbf{x}_\mathrm{r}\otimes\mathbf{m}_0^{-1}}\,\mathbf{E}^\mathrm{B} = \mathbf{Q}^{\llcorner}_{\mathbf{x}_\mathrm{r}}\,\mathbf{Q}^{\llcorner\top}_{\mathbf{m}_0}\,\mathbf{E}^\mathrm{B}\,. \tag{9}$$

Here, $\mathbf{E}^\mathrm{B}_\mathrm{r}$ denotes the basis preserving the Bingham principal directions $\mathbf{E}^\mathrm{B}$ transported from the mode $\mathbf{m}_0$ to $\mathbf{x}_\mathrm{r}$. The unit dual quaternion $\mathbf{x}_\mathrm{r}\otimes\mathbf{m}_0^{-1}$ denotes the difference between $\mathbf{m}_0$ and $\mathbf{x}_\mathrm{r}$. In fact, the column vectors of $\mathbf{E}^\mathrm{B}_\mathrm{r} = [\,\mathbf{e}^\mathrm{B}_1,\, \mathbf{e}^\mathrm{B}_2,\, \mathbf{e}^\mathrm{B}_3\,]$ can essentially be computed according to $\mathbf{e}^\mathrm{B}_i = \mathbf{x}_\mathrm{r} \otimes \mathbf{m}_0^{-1} \otimes \mathbf{m}_i$, meaning that the principal components $\{\mathbf{m}_i\}_{i=1}^3$ of the Bingham distribution are shifted jointly under the same 4-dimensional rotation $\mathbf{x}_\mathrm{r}\otimes\mathbf{m}_0^{-1}$. Therefore, $\{\mathbf{e}^\mathrm{B}_i\}_{i=1}^3$ provide an orthonormal basis for $\mathcal{T}_{\mathbf{x}_\mathrm{r}}\mathbb{S}^3$, i.e., $\mathcal{T}_{\mathbf{x}_\mathrm{r}}\mathbb{S}^3 = \mathrm{span}\,\{\mathbf{e}^\mathrm{B}_1,\, \mathbf{e}^\mathrm{B}_2,\, \mathbf{e}^\mathrm{B}_3\}$, which embodies the information geometry of the Bingham distribution at $\forall \mathbf{x}_\mathrm{r} \in \mathbb{S}^3$. With respect to the transported basis $\mathbf{E}_\mathrm{r}^\mathrm{B}$, the translation quaternion $\mathbf{x}_\mathrm{d}$ can be decoded into the following form

$$\mathbf{t}_\mathrm{B} = 2\,\mathbf{E}_\mathrm{r}^{\mathrm{B}\top}\mathbf{x}_\mathrm{d}\,, \tag{10}$$

such that $\mathbf{x}_\mathrm{d} = 0.5\,\mathbf{E}_\mathrm{r}^\mathrm{B}\,\mathbf{t}_\mathrm{B}$. By modeling $\mathbf{t}_\mathrm{B}$ with a certain distribution, e.g., a Gaussian distribution, that is uncorrelated to the real part, the true translation term encapsulated in the dual part defined in (6) shall be correlated with the real part.

C. Stochastic Modeling of Unit Dual Quaternions Based on Hyperspherical Geometry

The joint probability density function modeling the real and dual part of uncertain unit dual quaternions can be derived by marginalizing out the orientation-uncorrelated translation term $\mathbf{t}_\mathrm{B}$ of (10), namely

$$\begin{aligned} f(\mathbf{x}_\mathrm{r}, \mathbf{x}_\mathrm{d}) &= \int_{\mathbb{R}^3} f(\mathbf{x}_\mathrm{r}, \mathbf{x}_\mathrm{d}, \mathbf{t}_\mathrm{B})\, d\mathbf{t}_\mathrm{B} \\ &= \int_{\mathbb{R}^3} f(\mathbf{x}_\mathrm{r})\, f(\mathbf{x}_\mathrm{d}\,, \mathbf{t}_\mathrm{B} \,|\, \mathbf{x}_\mathrm{r})\, d\mathbf{t}_\mathrm{B} \\ &= f(\mathbf{x}_\mathrm{r}) \int_{\mathbb{R}^3} f(\mathbf{x}_\mathrm{d} \,|\, \mathbf{x}_\mathrm{r}, \mathbf{t}_\mathrm{B})\, f(\mathbf{t}_\mathrm{B} \,|\, \mathbf{x}_\mathrm{r})\, d\mathbf{t}_\mathrm{B} \\ &= f(\mathbf{x}_\mathrm{r}) \int_{\mathbb{R}^3} \delta(\mathbf{x}_\mathrm{d} - 0.5\,\mathbf{E}_\mathrm{r}^\mathrm{B}\,\mathbf{t}_\mathrm{B})\, f(\mathbf{t}_\mathrm{B})\, d\mathbf{t}_\mathrm{B} \\ &\propto f(\mathbf{x}_\mathrm{r})\, f(2\,\mathbf{E}_\mathrm{r}^{\mathrm{B}\top}\mathbf{x}_\mathrm{d})\,. \end{aligned} \tag{11}$$

Here, $\delta(\cdot)$ denotes the Dirac delta function which evaluates $f(\mathbf{t}_\mathrm{B})$ at $\mathbf{t}_\mathrm{B} = 2\mathbf{E}_\mathrm{r}^{\mathrm{B}\top}\mathbf{x}_\mathrm{d}$ according to (10) in the integral and results in the proportion [21, Theorem 265E]. We assume the real part to be Bingham-distributed, i.e., $\mathbf{x}_\mathrm{r} \sim \mathcal{B}(\mathbf{Z}, \mathbf{M})$, and the translation term $2\mathbf{E}_\mathrm{r}^{\mathrm{B}\top}\mathbf{x}_\mathrm{d}$ to be Gaussian-distributed with respect to the basis in (9), namely $2\mathbf{E}_\mathrm{r}^{\mathrm{B}\top}\mathbf{x}_\mathrm{d} \sim \mathcal{N}(\boldsymbol{\mu}\,, \boldsymbol{\Sigma})$. The second part can thus be derived as follows

$$\begin{aligned} &f(2\mathbf{E}_\mathrm{r}^{\mathrm{B}\top}\mathbf{x}_\mathrm{d}) \\ &\quad\propto \exp\big\{ -0.5\,(2\mathbf{E}_\mathrm{r}^{\mathrm{B}\top}\mathbf{x}_\mathrm{d} - \boldsymbol{\mu})^\top \boldsymbol{\Sigma}^{-1}(2\mathbf{E}_\mathrm{r}^{\mathrm{B}\top}\mathbf{x}_\mathrm{d} - \boldsymbol{\mu})\big\} \\ &\quad= \exp\Big\{ \big(\mathbf{x}_\mathrm{d} - \boldsymbol{\mu}_\mathrm{d}^\mathrm{r}\big)^\top \mathbf{C}_\mathrm{d}^\mathrm{r} \big(\mathbf{x}_\mathrm{d} - \boldsymbol{\mu}_\mathrm{d}^\mathrm{r}\big)\Big\}\,. \end{aligned}$$

Here, $\boldsymbol{\mu}_\mathrm{d}^\mathrm{r}$ indicates the dual part mean correlated to the real part and can be further derived given (9) as

$$\boldsymbol{\mu}_\mathrm{d}^\mathrm{r} = 0.5\,\mathbf{E}_\mathrm{r}^\mathrm{B}\boldsymbol{\mu} = 0.5\,\mathbf{Q}_{\mathbf{x}_\mathrm{r}}^{\llcorner}\,\mathbf{Q}_{\mathbf{m}_0}^{\llcorner\top}\,\mathbf{E}^\mathrm{B}\boldsymbol{\mu} = \mathbf{x}_\mathrm{r} \otimes \mathbf{m}_0^{-1} \otimes \boldsymbol{\mu}_\mathrm{d}\,,$$

with $\boldsymbol{\mu}_\mathrm{d} = 0.5\,\mathbf{E}^\mathrm{B}\boldsymbol{\mu} \in \mathcal{T}_{\mathbf{m}_0}\mathbb{S}^3$, which can be viewed as the mode of the dual part. As $\mathbf{m}_0^{-1} \otimes \boldsymbol{\mu}_\mathrm{d}$ is invariant to the orientation, the aforementioned equation can be further derived by applying the matrix representation in (3), such that

$$\boldsymbol{\mu}_\mathrm{d}^\mathrm{r} = \mathbf{Q}_{\mathbf{m}_0^{-1}\otimes\boldsymbol{\mu}_\mathrm{d}}^{\lrcorner}\,\mathbf{x}_\mathrm{r} = \mathbf{Q}_{\boldsymbol{\mu}_\mathrm{d}}^{\lrcorner}\,\mathbf{Q}_{\mathbf{m}_0}^{\lrcorner\top}\mathbf{x}_\mathrm{r} := \mathbf{T}_\mathrm{d}\,\mathbf{x}_\mathrm{r}\,,$$

with $\mathbf{T}_\mathrm{d} = \mathbf{Q}_{\boldsymbol{\mu}_\mathrm{d}}^{\lrcorner}\,\mathbf{Q}_{\mathbf{m}_0}^{\lrcorner\top}$ interpreting the correlation between rotation and translation quaternions. Meanwhile, we have

$$\begin{aligned} \mathbf{C}_\mathrm{d}^\mathrm{r} &= -2\mathbf{E}_\mathrm{r}^\mathrm{B}\,\boldsymbol{\Sigma}_\mathrm{t}^{-1}\mathbf{E}_\mathrm{r}^{\mathrm{B}\top} \\ &= -2\mathbf{Q}_{\mathbf{x}_\mathrm{r}}^{\llcorner}\,\mathbf{Q}_{\mathbf{m}_0}^{\llcorner\top}\,\mathbf{E}^\mathrm{B}\,\boldsymbol{\Sigma}_\mathrm{t}^{-1}\,\big(\mathbf{Q}_{\mathbf{x}_\mathrm{r}}^{\llcorner}\,\mathbf{Q}_{\mathbf{m}_0}^{\llcorner\top}\,\mathbf{E}^\mathrm{B}\big)^\top \\ &= -2\mathbf{Q}_{\mathbf{x}_\mathrm{r}}^{\llcorner}\,\mathbf{Q}_{\mathbf{m}_0}^{\llcorner\top}\,\mathbf{E}^\mathrm{B}\,\boldsymbol{\Sigma}_\mathrm{t}^{-1}\,\mathbf{E}^{\mathrm{B}\top}\mathbf{Q}_{\mathbf{m}_0}^{\llcorner}\,\mathbf{Q}_{\mathbf{x}_\mathrm{r}}^{\llcorner\top} \\ &:= \mathbf{Q}_{\mathbf{x}_\mathrm{r}}^{\llcorner}\,\mathbf{C}_\mathrm{d}\,\mathbf{Q}_{\mathbf{x}_\mathrm{r}}^{\llcorner\top}\,, \end{aligned}$$

Algorithm 1 Deterministic Sampling

procedure detSample$\,(\{\mathbf{Z}\,, \mathbf{M}\,, \boldsymbol{\mu}\,, \boldsymbol{\Sigma}\})$

1: $\{\mathbf{x}_\mathrm{r}^i, w_\mathrm{r}^i\}_{i=1}^n \leftarrow$ detSampleBingham$\,(\mathbf{Z}, \mathbf{M})$;
2: $\{\mathbf{t}_\mathrm{B}^j, w_\mathrm{t}^j\}_{j=1}^m \leftarrow$ detSampleGaussian$\,(\boldsymbol{\mu}\,, \boldsymbol{\Sigma})$;
3: $[\,\mathbf{E}^\mathrm{B}, \mathbf{m}_0\,] \leftarrow \mathbf{M}$;
4: $k \leftarrow 1$;
5: **for** $i = 1$ to n **do**
6: $\quad\mathbf{E}_{\mathrm{r},i}^\mathrm{B} \leftarrow \mathbf{Q}_{\mathbf{x}_\mathrm{r}^i}^{\llcorner}\,\mathbf{Q}_{\mathbf{m}_0}^{\llcorner\top}\,\mathbf{E}^\mathrm{B}$; // see (9)
7: $\quad$**for** $j = 1$ to m **do**
8: $\quad\quad\mathbf{x}_\mathrm{d}^{j|i} \leftarrow 0.5\,\mathbf{E}_{\mathrm{r},i}^\mathrm{B}\,\mathbf{t}_\mathrm{B}^j$;
9: $\quad\quad\mathbf{x}^k \leftarrow [\,\mathbf{x}_\mathrm{r}^{i\top}, \mathbf{x}_\mathrm{d}^{j|i\top}\,]^\top$;
10: $\quad\quad w^k \leftarrow w_\mathrm{r}^j \times w_\mathrm{t}^i$;
11: $\quad\quad k \leftarrow k + 1$;
12: $\quad$**end for**
13: **end for**
14: **return** $\{\mathbf{x}^k\,, w^k\}_{k=1}^{m\times n}$

end procedure

with $\mathbf{C}_\mathrm{d} = -2\,\mathbf{Q}_{\mathbf{m}_0}^{\llcorner\top}\,\mathbf{E}^\mathrm{B}\,\boldsymbol{\Sigma}_\mathrm{t}^{-1}\,\mathbf{E}^{\mathrm{B}\top}\mathbf{Q}_{\mathbf{m}_0}^{\llcorner}$ interpreting the orientation-invariant component of the dual part uncertainty. We can thus combine the Bingham-distributed real part and the conditioning Gaussian-distributed translation term according to (11) into the following concise form

$$\begin{aligned} f(\mathbf{x}) &\propto f_\mathcal{B}(\mathbf{x}_\mathrm{r})\, f_\mathcal{N}(2\,\mathbf{E}_\mathrm{r}^{\mathrm{B}\top}\mathbf{x}_\mathrm{d}) \\ &= \exp\big\{\mathbf{x}_\mathrm{r}^\top\mathbf{M}\,\mathbf{Z}\,\mathbf{M}^\top\mathbf{x}_\mathrm{r} - \\ &\quad 0.5\,(2\mathbf{E}_\mathrm{r}^{\mathrm{B}\top}\mathbf{x}_\mathrm{d} - \boldsymbol{\mu})^\top\boldsymbol{\Sigma}^{-1}\big(2\mathbf{E}_\mathrm{r}^{\mathrm{B}\top}\mathbf{x}_\mathrm{d} - \boldsymbol{\mu}\big)\big\} \\ &= \exp\big\{\mathbf{x}_\mathrm{r}^\top\mathbf{M}\,\mathbf{Z}\,\mathbf{M}^\top\mathbf{x}_\mathrm{r} + \\ &\quad (\mathbf{x}_\mathrm{d} - \mathbf{T}_\mathrm{d}\,\mathbf{x}_\mathrm{r})^\top\,\mathbf{Q}_{\mathbf{x}_\mathrm{r}}^{\llcorner}\,\mathbf{C}_\mathrm{d}\,\mathbf{Q}_{\mathbf{x}_\mathrm{r}}^{\llcorner\top}\,(\mathbf{x}_\mathrm{d} - \mathbf{T}_\mathrm{d}\,\mathbf{x}_\mathrm{r})\big\}\,. \end{aligned} \tag{12}$$

Moreover, the mode of the proposed distribution is

$$\mathbf{x}_\mathrm{mode} = \big[\,\mathbf{m}_0^\top\,, \boldsymbol{\mu}_\mathrm{d}^\top\,\big]^\top = \big[\,\mathbf{m}_0^\top,\, 0.5\,\boldsymbol{\mu}^\top\mathbf{E}^{\mathrm{B}\top}\,\big]^\top\,,$$

where the real part is the mode of the Bingham distribution and the dual part the Gaussian mean expressed in the basis composed by the Bingham principal directions.

IV. Unscented Pose Filtering

A. Deterministic Sampling and Parameter Fitting

In order to apply the proposed distribution for Bayesian inference, we further introduce a deterministic sampling scheme following the basic idea of unscented transform [22] (shown in Alg. 1 in detail). Given the parameters of the distribution $\{\mathbf{Z}\,, \mathbf{M}\,, \boldsymbol{\mu}\,, \boldsymbol{\Sigma}\}$ as introduced in Sec. III-C, deterministic samples are first drawn from the Bingham [9], [23] and the Gaussian part [22] individually. For each unit quaternion sample, we derive its associated tangent plane basis $\mathbf{E}_\mathrm{r}^\mathrm{B}$ according to (9), with respect to which the Gaussian samples are composed with the real part via (10), such that the dual part can be obtained (Alg. 1, line 6). Similarly, the weighting factors are computed through Cartesian product by multiplying the Bingham and Gaussian weights.

The aforementioned scheme can also be used for Monte Carlo-based random sampling processes. Here, we only need to substitute the deterministic samplings in line 1-2 of Alg. 1

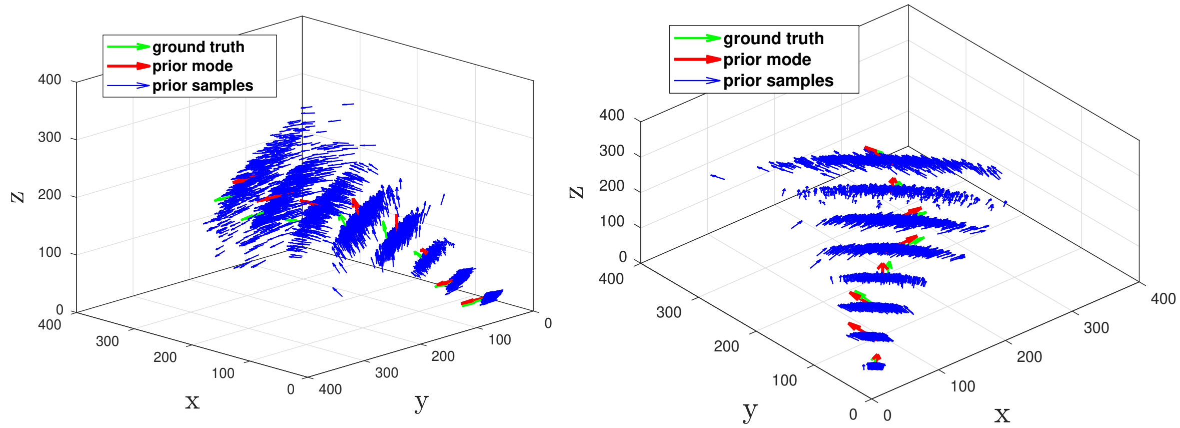

Fig. 3: Qualitative evaluation of unscented transform-based prediction steps using the proposed sampling-approximation scheme. The result is shown from two viewpoints. Here, the prediction steps are performed consecutively. Thus, the uncertainty dispersion gets larger as shown by the 6-DoF random samples (blue arrows) drawn continuously from the prior estimates. The proposed sampling-approximation scheme shows good performance for UT-based prediction.

Algorithm 2 Parameter Estimation

procedure estimateParameter $(\{\mathbf{x}^i, w^i\}_{i=1}^n)$
1: $\{\mathbf{M}, \mathbf{Z}\} \leftarrow$ estimateBingham $(\{\mathbf{x}_\mathrm{r}^i, w^i\}_{i=1}^n)$;
2: $[\,\mathbf{E}^\mathrm{B}, \mathbf{m}_0\,] \leftarrow \mathbf{M}$;
3: **for** $i = 1$ to n **do**
4: $\quad \mathbf{E}^\mathrm{B}_{\mathrm{r},i} \leftarrow \mathbf{Q}^\mathrm{L}_{\mathbf{x}_\mathrm{r}^i}\, \mathbf{Q}^{\mathrm{L}\top}_{\mathbf{m}_0}\, \mathbf{E}^\mathrm{B}$; // see (9)
5: $\quad \mathbf{t}_\mathrm{B}^i \leftarrow 2\, \mathbf{E}^{\mathrm{B}\top}_{\mathrm{r},i}\, \mathbf{x}_\mathrm{d}^i$;
6: **end for**
7: $\boldsymbol{\mu} \leftarrow \sum_{i=1}^n w^i\, \mathbf{t}_\mathrm{B}^i$;
8: $\boldsymbol{\Sigma} \leftarrow \sum_{i=1}^n w^i\, (\mathbf{t}_\mathrm{B}^i - \boldsymbol{\mu}_\mathrm{t}^\mathrm{B})\, (\mathbf{t}_\mathrm{B}^i - \boldsymbol{\mu}_\mathrm{t}^\mathrm{B})^\top$;
9: **return** $\{\, \mathbf{Z}\,, \mathbf{M}\,, \boldsymbol{\mu}\,, \boldsymbol{\Sigma}\,\}$
end procedure

with random ones [10]. Fig. 2 further shows results of random sampling on the proposed distribution under different parameter configurations. The dual quaternion samples are hereby visualized by 3-D quivers representing the spatial poses. Furthermore, the proposed distribution can also be re-approximated given weighted samples (shown in Alg. 2). Here, the Bingham component is first approximated by using the real parts of the dual quaternion samples as introduced in [9]. Based on the fitted Bingham parameters, we can therefore derive the tangent plane basis $\mathbf{E}_\mathrm{r}^\mathrm{B}$ corresponding to each quaternion sample, such that its uncorrelated translation term $\mathbf{t}_\mathrm{B}$ can be obtained (Alg. 2, line 4-5). The uncorrelated Gaussian parameters $\{\boldsymbol{\mu}, \boldsymbol{\Sigma}\}$ can thus be approximated from the collected $\mathbf{t}_\mathrm{B}$ samples (Alg. 2, line 7-8). We use the following example to show an application of the proposed sampling-approximation approach to Bayesian inference of uncertain system dynamics.

Example IV.1 *Our system model is:* $\mathbf{x}_k = \mathbf{x}_{k-1} \boxplus \mathbf{u}_{k-1} \boxplus \mathbf{v}_{k-1}$, *with* $\mathbf{x}_{k-1}\,, \mathbf{u}_{k-1}\,, \mathbf{v}_{k-1} \in \Omega$ *denoting the system state, input and noise, respectively. We assume the noise term* $\mathbf{v}_{k-1}$ *to be distributed according to the proposed density that is time-invariant. Therefore, the sampling-approximation scheme introduced in Alg. 1 and Alg. 2 can be practically integrated into an unscented transform (UT)-based prediction step, for instance, the one introduced in [24, Alg. 3]. Here, deterministic samples are drawn from the last prior estimate* f_{k-1}^p *and propagated with the noise samples drawn from the noise distribution* $f^\mathbf{v}$ *through Cartesian product. The current prior estimate* f_k^e *can therefore be obtained by re-approximating from the propagated samples. Fig. 3 shows the result for* 8 *consecutive prediction steps. The system input is given as a rotation of* $\theta = \pi/3$ *around axis* $\mathbf{n} = [\,1/\sqrt{3}, 1/\sqrt{3}, 1/\sqrt{3}\,]^\top$ *followed by a translation of* $\mathbf{t} = [\,30, 30, 30\,]^\top$.

B. Measurement Fusion

Without loss of generality, we assume the following formula for identity measurement models $\mathbf{z}_k = \mathbf{x}_k \boxplus \mathbf{w}_k$, with the noise term $\mathbf{w}_k \in \Omega$ following the proposed distribution. Thus, the posterior can be obtained according to Bayes' law as follows

$$f^\mathrm{e}(\mathbf{x}_k|\mathbf{z}_k) \propto \underbrace{f(\mathbf{z}_k|\mathbf{x}_k)}_{\text{likelihood}} \cdot \underbrace{f^\mathrm{p}(\mathbf{x}_k)}_{\text{prior}} \,.$$

By marginalizing out the noise term and further applying the definition of conditional probability, the likelihood can be reformulated into the following form

$$\begin{aligned} f(\mathbf{z}_k|\mathbf{x}_k) &= \int_\Omega f(\mathbf{z}_k, \mathbf{w}_k \,|\, \mathbf{x}_k)\, d\mathbf{w}_k \\ &= \int_\Omega f(\mathbf{z}_k \,|\, \mathbf{w}_k, \mathbf{x}_k)\, f(\mathbf{w}_k)\, d\mathbf{w}_k \\ &= \int_\Omega \delta(\mathbf{w}_k - \mathbf{z}_k \boxplus \mathbf{x}_k^{-1})\, f(\mathbf{w}_k)\, d\mathbf{w}_k \\ &= f^\mathbf{w}(\mathbf{z}_k \boxplus \mathbf{x}_k^{-1})\,, \end{aligned}$$

which is the noise density evaluated at the unit dual quaternion indicating the difference between the measurement and the prior. By applying the arithmetics of unit dual quaternions introduced in Sec. II, the difference term can be derived as [2]

$$\mathbf{x}^{-1} \boxplus \mathbf{z} = \begin{bmatrix} \mathbf{x}_\mathrm{r}^{-1} \otimes \mathbf{z}_\mathrm{r} \\ \mathbf{x}_\mathrm{r}^{-1} \otimes \mathbf{z}_\mathrm{d} + \mathbf{x}_\mathrm{d}^* \otimes \mathbf{z}_\mathrm{r} \end{bmatrix} := \begin{bmatrix} \Delta_\mathrm{r} \\ \Delta_\mathrm{d} \end{bmatrix} .$$

[2]For better readability of the algorithm, we ignore the time stamp index k of the state and measurement variable $\mathbf{x}_k$ and $\mathbf{z}_k$.

Algorithm 3 Measurement Fusion

procedure fuseMeasurement$(f^{\mathrm{p}}, f^{\mathbf{w}}, \mathbf{z})$

1: $[\mathbf{z}_{\mathrm{r}}^\top, \mathbf{z}_{\mathrm{d}}^\top]^\top \leftarrow \mathbf{z}$;

2: $f_{\mathcal{B}}^{\mathrm{e}} \leftarrow$ fuseBingham $(f_{\mathcal{B}}^{\mathrm{p}}, f_{\mathcal{B}}^{\mathbf{w}}, \mathbf{z}_{\mathrm{r}})$; // see [9]

3: $\{\mathbf{Z}^{\mathrm{e}}, \mathbf{M}^{\mathrm{e}}\} \leftarrow f_{\mathcal{B}}^{\mathrm{e}}$;

4: $f_{\mathcal{N}}^{\mathrm{e}} \leftarrow f_{\mathcal{N}}^{\mathrm{p}}$;

5: $\{\boldsymbol{\mu}^{\mathbf{w}}, \boldsymbol{\Sigma}^{\mathbf{w}}\} \leftarrow f_{\mathcal{N}}^{\mathbf{w}}$;

6: $\{\mathbf{x}_{\mathrm{r}}^i\}_{i=1}^n \leftarrow$ detSampling $(\mathbf{Z}^{\mathrm{e}}, \mathbf{M}^{\mathrm{e}})$; // see [23]

7: **for** $i = 1$ to n **do**

8: $\quad \mathbf{E}_{\mathrm{r},i}^{\mathrm{B}} \leftarrow \mathbf{Q}_{\mathbf{x}_{\mathrm{r}}^i}^{\llcorner} \, \mathbf{Q}_{\mathbf{m}_0}^{\llcorner\top} \, \mathbf{E}^{\mathrm{B}}$; // see (9)

9: $\quad \mathbf{t}_{\mathrm{B}} \leftarrow 2\, \mathbf{E}_{\mathrm{r},i}^{\mathrm{B}\top} \mathbf{z}_{\mathrm{d}}$;

10: $\quad f_{\mathcal{N}}^{\mathrm{e}} \leftarrow$ updateKF $(f_{\mathcal{N}}^{\mathrm{e}}, f_{\mathcal{N}}^{\mathbf{w}}, \mathbf{t}_{\mathrm{B}})$;

11: **end for**

12: $\{\boldsymbol{\mu}^{\mathrm{e}}, \boldsymbol{\Sigma}^{\mathrm{e}}\} \leftarrow f_{\mathcal{N}}^{\mathrm{e}}$;

13: **return** $\{\mathbf{Z}^{\mathrm{e}}, \mathbf{M}^{\mathrm{e}}, \boldsymbol{\mu}^{\mathrm{e}}, \boldsymbol{\Sigma}^{\mathrm{e}}\}$

end procedure

Unlike in the case of planar motions introduced in [10], [24], $[\Delta_{\mathrm{r}}^\top, \Delta_{\mathrm{d}}^\top]^\top$ cannot be trivially turned into a closed-form update step for the proposed distribution. However, since the distribution in (12) is given as the product of the Bingham and the orientation-invariant Gaussian, the real part Δ_{r} can still be fused in closed form [9]. In order to fuse the measurement of the dual part in a coherent way, we propose an unscented transform-based fusion approach, as shown in Alg. 3 in detail. Here, the Bingham part is first updated in closed form as mentioned in [9]. We then draw quaternion samples deterministically from the Bingham part and traverse each of their associated tangent planes, on which an ordinary Kalman filter (KF) update step is performed for the Gaussian part (Alg. 3, line 8-10). As the Gaussian part is updated sequentially throughout all the sampled tangent planes, the quaternion samples should be equally weighted. It is thus recommended to employ deterministic Bingham sampling approaches proposed in [23], [25], which guarantees equal weighting factors. The following example shows a quantitative evaluation of the proposed measurement fusion method.

Example IV.2 *We use the measurement model setup in Sec. IV-B with the prior and measurement noise distribution given as*

- $\mathbf{C}_{\mathcal{B}}^{p} = -\mathrm{diag}(1, 500, 500, 500)$, $\boldsymbol{\Sigma}_{\mathcal{N}}^{p} = 0.001 \times \mathbf{I}$;
- $\mathbf{C}_{\mathcal{B}}^{\mathbf{w}} = -\mathrm{diag}(1, 1/a, 2/a, 3/a)$, $\boldsymbol{\Sigma}_{\mathcal{N}}^{\mathbf{w}} = a \times \mathbf{I}$.

Here, a is selected from $\{0, 1, 0.01, 0.001\}$ and is used to control the measurement noise level, with a larger value indicating higher noise level for both the Bingham and Gaussian parts. The Bingham parameters $\mathbf{C}_{\mathcal{B}}^{\mathbf{w}}$ and $\mathbf{C}_{\mathcal{B}}^{p}$ are given in the concise form as mentioned in Sec. II-C, indicating both modes at $[1, 0, 0, 0]^\top$. The Gaussian terms are also zero-centered with the identity matrix $\mathbf{I} \in \mathbb{R}^{3\times3}$. Here, a hidden state $\mathbf{x}_{gt}$ incorporating a noise term $\mathbf{v}$ is given as the ground truth. It is generated via $\mathbf{x}_{gt} = \mathbf{u} \boxplus \mathbf{v}$, with $\mathbf{v}$ also distributed according to the proposed distribution parameterized as follows

- $\mathbf{C}_{\mathcal{B}}^{\mathbf{v}} = -\mathrm{diag}(1, 400, 400, 400)$, $\boldsymbol{\Sigma}_{\mathcal{N}}^{\mathbf{v}} = 0.002 \times \mathbf{I}$.

Here, the noise for the hidden state is also zero-centered (same as the prior). Therefore, we use $\mathbf{u} \in \Omega$ as a shifting term to diverge the ground truth away from the mode of the prior. The $\mathbf{u}$ encodes a rotation of degree $\theta = \pi/3$ around axis $\mathbf{n} = 1/\sqrt{3} \times [1, 1, 1]^\top$ followed by a translation of $\mathbf{t} = [5, 4, 6]^\top$.

In the simulation, we generate the hidden state $\mathbf{x}_{gt}$ by propagating $\mathbf{u}$ with one random sample $\mathbf{v}$ drawn from $f^{\mathbf{v}}$. The prior f^p is then updated by sequentially fusing measurements generated via $\mathbf{z} = \mathbf{x}_{gt} \boxplus \mathbf{w}$, with $\mathbf{w}$ randomly drawn from the measurement noise distribution $f^{\mathbf{w}}$ each time. Fig. 4 shows the results of 50 sequential update steps by using the measurement fusion approach in Alg. 3. For all of the noise levels considered, both rotation and translation errors decrease with growing fusion steps. With lower noise level (smaller a), the posterior estimate converges faster towards the ground truth.

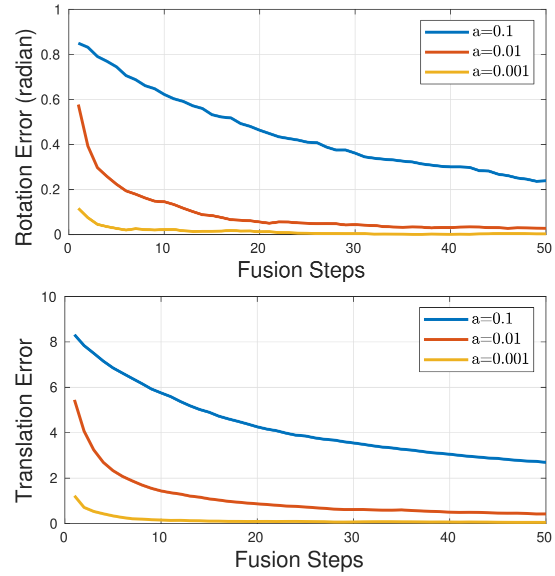

Fig. 4: Evaluation of sequential updates using the proposed measurement fusion methods in Sec. IV-B . Here, the representative run is shown.

V. Conclusion

In this paper, a novel approach is proposed to stochastically model uncertain 6-DoF rigid body motions represented by unit dual quaternions. The resulting distribution is directly defined on the manifold of unit dual quaternions without local linearizations, inherently considering the nonlinearity of the underlying group. Besides, by applying the parallel transport technique from Riemannian geometry to the Bingham distribution on the $\mathbb{S}^3$ hypersphere, a probabilistic interpretation of the correlation between the rotation and translation terms is enabled. A corresponding sampling-approximation scheme is also proposed and employed further in an unscented transform-based pose filtering framework. However, there is much potential to exploit from the proposed work. First, it might be possible to simplify the distribution parameters into a more concise form, e.g., a single 8×8 matrix. Second, it is of interest to evaluate the proposed unscented filtering approaches for real-world applications, e.g., robotic pose estimation and perception, localization in sensor networks [26], etc.

Appendix

A. Matrix Representation of Unit Quaternions

$\forall\,\mathbf{p},\,\mathbf{q}\in\mathbb{S}^3$, $\mathbf{p}\otimes\mathbf{q}=\mathbf{Q}^{\llcorner}_{\mathbf{p}}\,\mathbf{q}$, with $\mathbf{Q}^{\llcorner}_{\mathbf{p}}$ as given in (3). Since $\mathbf{p}=[\,p_1,p_2,p_3,p_4\,]^\top\in\mathbb{S}^3$, we have $\mathbf{Q}^{\llcorner\top}_{\mathbf{p}}\mathbf{Q}^{\llcorner}_{\mathbf{p}}=\mathbf{Q}^{\llcorner}_{\mathbf{p}}\,\mathbf{Q}^{\llcorner\top}_{\mathbf{p}}=\mathbf{I}\in\mathbb{R}^{4\times 4}$ and $\det(\mathbf{Q}^{\llcorner}_{\mathbf{p}})=1$, thus $\mathbf{Q}^{\llcorner}_{\mathbf{p}}\in\mathrm{SO}(4)$, i.e., the 4-dimensional group. Similarly, it can be proven that in (3) the right matrix representation $\mathbf{Q}^{\lrcorner}_{\mathbf{q}}\in\mathrm{SO}(4)$.

B. Dual Quaternion Product

The product of two dual quaternions can be derived as $\mathbf{x}^1\boxplus\mathbf{x}^2=(\mathbf{x}^1_\mathrm{r}+\epsilon\,\mathbf{x}^1_\mathrm{d})(\mathbf{x}^2_\mathrm{r}+\epsilon\,\mathbf{x}^2_\mathrm{d})=\mathbf{x}^1_\mathrm{r}\otimes\mathbf{x}^2_\mathrm{r}+\epsilon\,(\mathbf{x}^1_\mathrm{r}\otimes\mathbf{x}^2_\mathrm{d}+\mathbf{x}^1_\mathrm{d}\otimes\mathbf{x}^2_\mathrm{r})+\epsilon^2\,\mathbf{x}^1_\mathrm{d}\otimes\mathbf{x}^2_\mathrm{d}=\mathbf{x}^1_\mathrm{r}\otimes\mathbf{x}^2_\mathrm{r}+\epsilon\,(\mathbf{x}^1_\mathrm{r}\otimes\mathbf{x}^2_\mathrm{d}+\mathbf{x}^1_\mathrm{d}\otimes\mathbf{x}^2_\mathrm{r})\,.$

C. Dual Quaternions of Unit Norm

The squared norm of a dual quaternion $\mathbf{x}=\mathbf{x}_\mathrm{r}+\epsilon\,\mathbf{x}_\mathrm{d}$ can be derived by exploiting $\epsilon^2=0$ as $\mathbf{x}\boxplus\mathbf{x}^*=(\mathbf{x}_\mathrm{r}+\epsilon\,\mathbf{x}_\mathrm{d})(\mathbf{x}^*_\mathrm{r}+\epsilon\,\mathbf{x}^*_\mathrm{d})=\mathbf{x}_\mathrm{r}\otimes\mathbf{x}^*_\mathrm{r}+\epsilon\,(\mathbf{x}_\mathrm{r}\otimes\mathbf{x}^*_\mathrm{d}+\mathbf{x}_\mathrm{d}\otimes\mathbf{x}^*_\mathrm{r})=\mathbf{x}_\mathrm{r}\otimes\mathbf{x}^*_\mathrm{r}+\epsilon\,(\mathbf{x}_\mathrm{r}\otimes\mathbf{x}^*_\mathrm{d}+(\mathbf{x}_\mathrm{r}\otimes\mathbf{x}^*_\mathrm{d})^*)\,$. The dual part in the aforementioned form is thus the sum of quaternion $\mathbf{x}_\mathrm{r}\otimes\mathbf{x}^*_\mathrm{d}$ with its own conjugate. According to the Hamilton product in (3), this leads to a scalar value, namely $\mathbf{x}_\mathrm{r}\otimes\mathbf{x}^*_\mathrm{d}+(\mathbf{x}_\mathrm{r}\otimes\mathbf{x}^*_\mathrm{d})^*=2\,\mathbf{x}_\mathrm{r}^\top\mathbf{x}_\mathrm{d}\,$. Thus, we have $\mathbf{x}\boxplus\mathbf{x}^*=\mathbf{x}_\mathrm{r}\otimes\mathbf{x}^*_\mathrm{r}+2\,\epsilon\,\mathbf{x}_\mathrm{r}^\top\mathbf{x}_\mathrm{d}$ to fulfill the unit norm constraint, i.e., $\|\mathbf{x}\|=\sqrt{\mathbf{x}\boxplus\mathbf{x}^*}=1$, which results in the manifold of unit dual quaternions as shown in (5).

D. Spatial Transformations via Unit Dual Quaternions

For any $\mathbf{v}\in\mathbb{R}^3$, it can be transformed by a unit dual quaternion to $\mathbf{v}'$ according to (7) as follows

$$
\begin{aligned}
&\mathbf{x}\boxplus[\,1,0,0,0,0,\mathbf{v}^\top\,]^\top\boxplus\mathbf{x}^\circ\\
&=(\mathbf{x}_\mathrm{r}+\epsilon\,\mathbf{x}_\mathrm{d})([\,1,0,0,0\,]^\top+\epsilon\,[\,0,\mathbf{v}^\top\,]^\top)(\mathbf{x}^*_\mathrm{r}-\epsilon\,\mathbf{x}^*_\mathrm{d})\\
&=(\mathbf{x}_\mathrm{r}+\epsilon\,\mathbf{x}_\mathrm{r}\otimes[\,0,\mathbf{v}^\top\,]^\top+\epsilon\,\mathbf{x}_\mathrm{d})(\mathbf{x}^*_\mathrm{r}-\epsilon\,\mathbf{x}^*_\mathrm{d})\\
&=\mathbf{x}_\mathrm{r}\otimes\mathbf{x}^*_\mathrm{r}-\epsilon\,(\mathbf{x}_\mathrm{r}\otimes\mathbf{x}^*_\mathrm{d}-\mathbf{x}_\mathrm{r}\otimes[\,0,\mathbf{v}^\top\,]^\top\otimes\mathbf{x}^*_\mathrm{r}-\mathbf{x}_\mathrm{d}\otimes\mathbf{x}^*_\mathrm{r})
\end{aligned}
$$

As $\mathbf{x}_\mathrm{r}\otimes\mathbf{x}^*_\mathrm{d}=(\mathbf{x}_\mathrm{d}\otimes\mathbf{x}^*_\mathrm{r})^*$ and $\mathbf{x}_\mathrm{d}\otimes\mathbf{x}^*_\mathrm{r}=\mathbf{x}_\mathrm{d}\otimes\mathbf{x}^{-1}_\mathrm{r}=0.5\,[\,0,\mathbf{t}^\top\,]^\top$, it can be further derived that $\mathbf{x}_\mathrm{r}\otimes\mathbf{x}^*_\mathrm{d}-\mathbf{x}_\mathrm{d}\otimes\mathbf{x}^*_\mathrm{r}=-[\,0,\mathbf{t}^\top\,]^\top$. Given $\mathbf{x}_\mathrm{r}\otimes\mathbf{x}^*_\mathrm{r}=[\,1,0,0,0\,]^\top$, we have

$$
\begin{aligned}
&\mathbf{x}\boxplus[\,1,0,0,0,0,\mathbf{v}^\top\,]^\top\boxplus\mathbf{x}^\circ\\
&=[\,1,0,0,0\,]^\top+\epsilon(\mathbf{x}_\mathrm{r}\otimes[\,0,\mathbf{v}^\top\,]^\top\otimes\mathbf{x}^*_\mathrm{r}+[\,0,\mathbf{t}^\top\,]^\top)\,,
\end{aligned}
$$

resulting in a transformation of rotation via $\mathbf{x}_\mathrm{r}$ followed by a translation of $\mathbf{t}$, namely $[\,0,\mathbf{v}'^\top\,]^\top=\mathbf{x}_\mathrm{r}\otimes[\,0,\mathbf{v}^\top\,]^\top\otimes\mathbf{x}^*_\mathrm{r}+[\,0,\mathbf{t}^\top\,]^\top$.

Acknowledgment

This work is supported by the German Research Foundation (DFG) under grant HA 3789/16-1.

References

[1] K. Li, G. Kurz, L. Bernreiter, and U. D. Hanebeck, "Simultaneous Localization and Mapping Using a Novel Dual Quaternion Particle Filter," in *Proceedings of the 21st International Conference on Information Fusion (Fusion 2018)*, Cambridge, United Kingdom, Jul. 2018.

[2] A. Byravan and D. Fox, "SE3-Nets: Learning Rigid Body Motion Using Deep Neural Networks," in *Proceedings of the 2017 IEEE International Conference on Robotics and Automation (ICRA 2017)*, 2017, pp. 173–180.

[3] J. Civera, O. G. Grasa, A. J. Davison, and J. Montiel, "1-Point RANSAC for Extended Kalman Filtering: Application to Real-time Structure from Motion and Visual Odometry," *Journal of Field Robotics*, vol. 27, no. 5, pp. 609–631, 2010.

[4] T. Klamt, D. Rodriguez, M. Schwarz, C. Lenz, D. Pavlichenko, D. Droeschel, and S. Behnke, "Supervised Autonomous Locomotion and Manipulation for Disaster Response with a Centaur-like Robot," in *Proceedings of the 2018 IEEE/RSJ International Conference on Intelligent Robots and Systems (IROS 2018)*, 2018.

[5] M. Brossard, S. Bonnabel, and J.-P. Condomines, "Unscented Kalman Filtering on Lie groups," in *Proceedings of the 2017 IEEE/RSJ International Conference on Intelligent Robots and Systems (IROS 2017)*, 2017, pp. 2485–2491.

[6] M. Bloesch, M. Burri, S. Omari, M. Hutter, and R. Siegwart, "Iterated Extended Kalman Filter Based Visual-inertial Odometry Using Direct Photometric Feedback," *The International Journal of Robotics Research*, vol. 36, no. 10, pp. 1053–1072, 2017.

[7] J. Brookshire and S. Teller, "Extrinsic Calibration From Per-sensor Egomotion," *Robotics: Science and Systems VIII*, pp. 504–512, 2013.

[8] J. Glover, G. Bradksi, and R. Rusu, "Monte Carlo Pose Estimation with Quaternion Kernels and the Bingham Distribution," in *Robotics: Science and Systems*, 2011.

[9] I. Gilitschenski, G. Kurz, S. J. Julier, and U. D. Hanebeck, "Unscented Orientation Estimation Based on the Bingham Distribution," *IEEE Transactions on Automatic Control*, vol. 61, no. 1, pp. 172–177, Jan. 2016.

[10] ——, "A New Probability Distribution for Simultaneous Representation of Uncertain Position and Orientation," in *Proceedings of the 17th International Conference on Information Fusion (Fusion 2014)*, Salamanca, Spain, Jul. 2014.

[11] K. Li, G. Kurz, L. Bernreiter, and U. D. Hanebeck, "Nonlinear Progressive Filtering for SE(2) Estimation," in *Proceedings of the 21st International Conference on Information Fusion (Fusion 2018)*, Cambridge, United Kingdom, Jul. 2018.

[12] R. A. Srivatsan, G. T. Rosen, D. F. N. Mohamed, and H. Choset, "Estimating SE(3) Elements Using a Dual Quaternion Based Linear Kalman Filter." in *Robotics: Science and Systems*, 2016.

[13] S. Bultmann, K. Li, and U. D. Hanebeck, "Stereo Visual SLAM Based on Unscented Dual Quaternion Filtering (submitted)," in *Proceedings of the 22st International Conference on Information Fusion (Fusion 2019)*, Ottawa, Canada, Jul. 2019.

[14] W. Feiten and M. Lang, "MPG-A Framework for Reasoning on 6 DOF Pose Uncertainty," *arXiv preprint arXiv:1707.01941*, 2017.

[15] S. Amari and H. Nagaoka, *Methods of Information Geometry*. American Mathematical Soc., 2007, vol. 191.

[16] K. Li, D. Frisch, S. Radtke, B. Noack, and U. D. Hanebeck, "Wavefront Orientation Estimation Based on Progressive Bingham Filtering," in *Proceedings of the IEEE ISIF Workshop on Sensor Data Fusion: Trends, Solutions, Applications (SDF 2018)*, Oct. 2018.

[17] W. R. Hamilton, "On Quaternions; or on a New System of Imaginaries in Algebra," *Philosophical Magazine Series 3*, vol. 25, no. 163, pp. 10–13, 1844.

[18] C. Bingham, "An Antipodally Symmetric Distribution on the Sphere," *Ann. Statist.*, vol. 2, no. 6, pp. 1201–1225, 11 1974.

[19] M. P. do Carmo, *Riemannian Geometry*. Birkhäuser, 1992.

[20] B. Busam, T. Birdal, and N. Navab, "Camera Pose Filtering with Local Regression Geodesics on the Riemannian Manifold of Dual Quaternions," *arXiv preprint arXiv:1704.07072*, 2017.

[21] D. H. Fremlin, *Measure Theory Volume 2*, 2001.

[22] E. A. Wan and R. V. D. Merwe, "The Unscented Kalman Filter for Nonlinear Estimation," in *Proceedings of the IEEE 2000 Adaptive Systems for Signal Processing, Communications, and Control Symposium (Cat. No.00EX373)*, Oct 2000, pp. 153–158.

[23] K. Li, D. Frisch, B. Noack, and U. D. Hanebeck, "Geometry-driven Deterministic Sampling for Nonlinear Bingham Filtering," in *Proceedings of the 2019 European Control Conference (ECC 2019)*, Naples, Italy, Jun. 2019.

[24] I. Gilitschenski, G. Kurz, and U. D. Hanebeck, "A Stochastic Filter for Planar Rigid-Body Motions," in *Proceedings of the 2015 IEEE International Conference on Multisensor Fusion and Integration for Intelligent Systems (MFI 2015)*, San Diego, California, USA, Sep. 2015.

[25] K. Li, F. Pfaff, and U. D. Hanebeck, "Hyperspherical Deterministic Sampling Based on Riemannian Geometry for Improved Nonlinear Bingham Filtering (submitted)," in *Proceedings of the 22st International Conference on Information Fusion (Fusion 2019)*, Ottawa, Canada, Jul. 2019.

[26] S. Radtke, K. Li, B. Noack, and U. D. Hanebeck, "Comparative Study of Track-to-Track Fusion Methods for Cooperative Tracking with Bearing-only Measurements," in *Proceedings of the 2019 IEEE International Conference on Multisensor Fusion and Integration for Intelligent Systems (MFI 2019)*, Taipei, Republic of China, May 2019.